Solar Panel Efficiency and Visible Light Detection on High-Altitude Balloons

Maxim Somov[a], Sujay Venuganti[a]

Abstract

Experiments designed for high-altitude balloon (HAB) payloads often require some source of electrical power. This design constraint is usually satisfied with consumer-grade batteries such as zinc-carbon dry cells or lithium-ion polymer batteries. This paper explores the feasibility of using small form factor consumer-grade solar panels as a supplementary way to provide this electrical power and the corresponding challenges associated with their introduction. Test flights were conducted with two 2.36-inch by 3.54-inch polysilicon solar panels mounted bilaterally on a 3D-printed payload structure. The corresponding voltages and currents produced by the panels were recorded throughout the high-altitude balloon flight. To record the ambient conditions, luminosity sensors were also mounted in-plane with the solar panels on both sides, and an environmental sensor was used to measure the ambient pressure, temperature, and humidity. In addition to helping analyze the ambient atmospheric conditions, the luminosity sensors also helped normalize the light conditions and readily compare the power generation at different altitudes. Test flights to record data were done in both daylight conditions as well as the 2024 total solar eclipse. Preliminary data suggests that solar panels may be a useful supplement for power generation on sun-incandescent high-altitude ballooning flights.

Solar Panels | Luminosity | Voltage | Current | 3D-Printing | Total Solar Eclipse | Power Generation

1. Introduction

The first part of this study experimentally determines the voltage and current across small consumer-grade polysilicon solar panels during the ascent stage of a high-altitude balloon flight. The following section examines the use of luminosity sensors to measure the amount of visible light (400nm-700nm) during the ascent stage of a high-altitude balloon. The luminosity values are then compared to the amount of voltage and current across the solar panels during the same exact time instant. Finally, the paper explores the feasibility of implementing solar panels onto high-altitude balloon payloads and discusses the associated challenges and benefits related to their introduction.

The objectives discussed were achieved by building a custom payload structure out of 3D-printed components and consumer-grade electronics. Two solar panels and luminosity sensors were mounted bilaterally on the payload structure at a 15-degree decline relative to the payload structure horizon and a flight computer recorded the corresponding voltage, current, and luminosity during the flight. The payload structure was attached to the high-altitude balloon using a nylon flight string that ran through its center shaft. The payload was flown as part of the High-Altitude Ballooning at Virginia Tech (HAB@VT) design team and was launched on two different occasions. The first flight of the payload occurred on February 24, 2024, and recorded roughly 31 minutes of useful data. The next flight opportunity occurred on April 8, 2024, and

[a]Undergraduate student, Virginia Polytechnic Institute and State University, Blacksburg, VA

recorded about 51 minutes worth of data. To record the voltage and current across the solar panels, the team utilized an INA219 power monitoring module programmed to read the values at 50Hz and save the last recording to an Adafruit Feather M0 Adalogger in 1-second intervals. The data was then recovered after the payload was found and then analyzed by the team using Python alongside the open-source matplotlib library. The payload also had a VEML7700 ambient light sensor which recorded data at 40Hz and saved the last recording to the Adalogger at 1-second intervals. The theoretical background used for this experiment is found in the succeeding section:

1.1. Solar Panel Theory

The first technology analyzed by the team in this study is solar panels. The team used a type of solar panel known as polycrystalline. These solar panels are manufactured by melting together pieces of silicon crystals to form one single wafer. This process allows for a cheaper solar panel in exchange for performance tradeoffs. The other type of solar panel, monocrystalline, on the other hand, is manufactured from a single silicon crystal to form a single, more efficient, wafer [1]. Once a solar panel is selected and configured, it can then be used to produce power for various electronic applications. Visible light, between 400 nm and 700 nm, is absorbed by the silicon wafer to produce an electric potential (voltage) which then allows for current to flow. As such, solar panels essentially act as power sources in a similar fashion as batteries.

1.2. Luminosity Sensor Theory

As discussed above, solar panel power generation is directly related to the amount of visible light seen by the solar panel. As a result, the team decided to also implement luminosity sensors in-plane with the solar panels to record the corresponding brightness. The luminosity sensors work by utilizing a high-sensitivity photodiode that produces a current corresponding to the amount of visible light that hits the active area. An amplifying circuit then scales this current and matches it to a corresponding luminosity value [2].

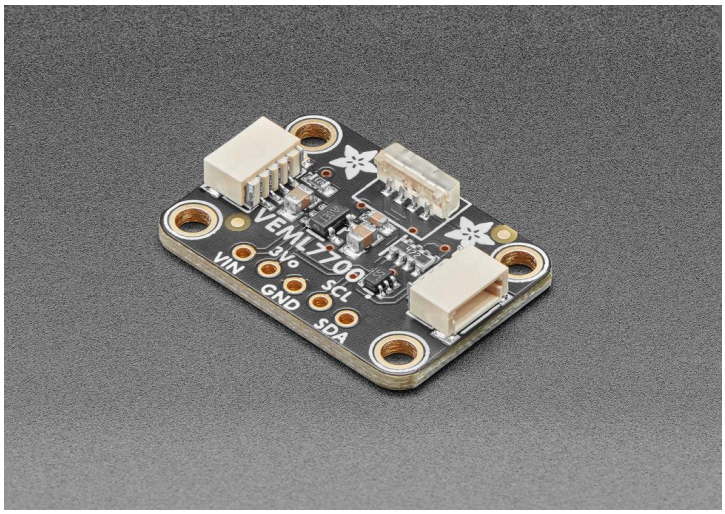

Fig. 1. VEML7700 I2C Luminosity Sensor used to quantify the amount of light detected by the solar panel [3].

1.3. Report Overview

This report will be organized in the following structure. Following a brief technical background, the payload structure and sensors used in the experiment are then detailed, including information on the balloon flights and the associated uncertainties with the study. Observations and discussions are made based on the recorded data from the flights, and conclusions are drawn based on the data and its trends.

2. Structure and Electronics

2.1. Payload Structure

A custom payload structure was designed to mount the solar panels and luminosity sensors. This structure was initially modeled using Siemens NX CAD software and then manufactured, assembled, and tested at the HAB@VT laboratory. Figure 2 illustrates a complete rendering of the structure. For manufacturing, the structure was divided into 12 unique components comprising a total of 19 pieces. Each component was 3D printed using polylactic acid (PLA) plastic on an Ender-3 3D printer. The density of the components varied: non-critical parts like wire guides were printed at 20% density, while critical parts such as the walls and solar panel mounts were printed at 100% density. After 3D printing, the components were assembled using brass threaded inserts, which were heat-set into the plastic. The pieces were then put together with M2.5 and M3 screws. Additionally, the flight string was threaded through the center of the structure and secured with knots on both ends.

The two critical pieces of this structure related to the study are the two bilaterally mounted solar panel holders that are seen in Figure 3. In Figure 3, a 2.36-inch by 3.54-inch rectangular plane is visible to which a solar panel is attached. Below this rectangular plane, there is a mounting point for a VEML7700 luminosity sensor. The solar panel was mounted using double-sided adhesive tape while the VEML7700 was secured using M2.5 screws. Figure 4 then shows a 15-degree angle at which the solar panels are declined. This angle was chosen by the team to prevent shadows from payloads above this payload from interfering with the light detection. Figure 5 shows the final manufactured structure that was flown on the two flights. It is also important to note that the payload structure was placed inside a styrofoam box following assembly to increase heat retention and prevent the batteries or the main flight computer from freezing. The box is 6.5 inches by 8 inches and has a uniform wall thickness of about 1 inch.

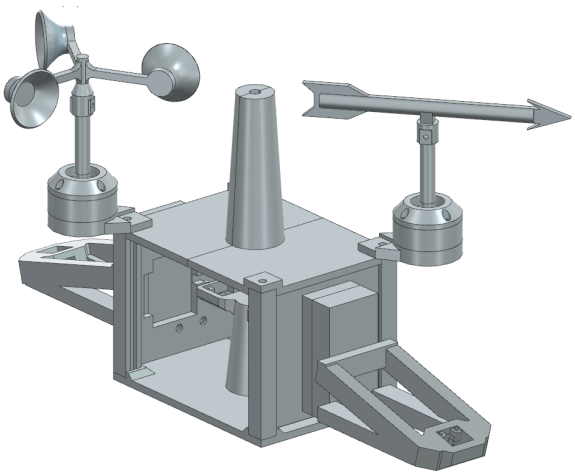

Fig. 2. 3D render of the payload structure.

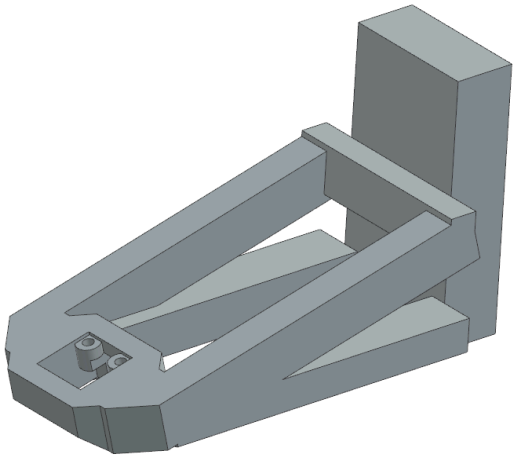

Fig. 3. 3D render of solar panel and luminosity sensor holders.

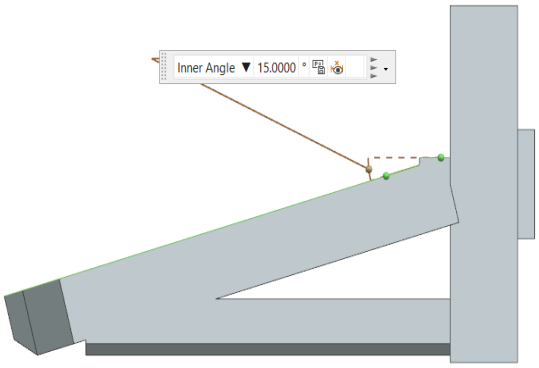

Fig. 4. Side view of solar panel and luminosity sensor holders with a 15-degree decline relative to the local horizontal.

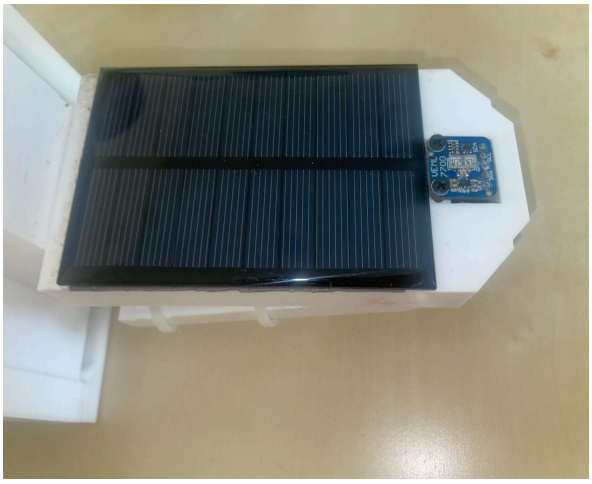

Fig. 5. Assembled solar panel and luminosity sensor in HAB@VT laboratory.

2.2. Main Payload Electronics

To carry out the study, the team purchased and wired multiple sensors within the payload structure. The solar panels used in the investigation are the Treedix 5V 150ma polysilicon solar panels that are 2.36-inch by 3.54-inch in size and encapsulated in a waterproof resin. The team selected these solar panels due to their small size and low cost. It is important to note that the solar panels were not used to power any electronics on the payload. To record the current and voltage across the sensors an INA219 power supply sensor module was used. The sensor is manufactured by HiLetgo and uses the I2C communication protocol to communicate with the main onboard computer. The INA219 has a programmable precision amplifier that was used by the team to record current at ±400mA with a resolution of 0.1mA. The sensor also offers a +26VDC range to measure the high-side voltage across a device. The sensor was pinged using

the I2C protocol every 20ms for a frequency of 50Hz [4]. Next, there are the luminosity sensors. The sensor selected by the team was a VEML7700 ambient light sensor manufactured by HiLetgo. These sensors are rated "0 lx to about 140 klx" with a "resolution down to 0.0042 lx/ct" [2]. These sensors also use the I2C communication protocol and were pinged every 25ms for a frequency of 40Hz.

2.3. Additional Electronics

To control the aforementioned payload sensors, the team utilized an Adafruit Feather M0 Adalogger as the main flight computer. The Adalogger has a built-in micro SD card breakout which the team utilized to save the data onto a SanDisk 32GB micro SD card. Saving of data was done every 1 second after the initial calibration of the payload was complete. To program the flight computer and sensors, Arduino C was used alongside many open-source libraries and packages. Because multiple INA219 and VEML7700 sensors were used on the payload, a problem with the I2C protocol arose where identical sensors had the same I2C address. To address this problem, the team introduced a HiLetgo TCA9548A I2C multiplexer. This multiplexer allowed the team to communicate with identical sensors using pre-defined built-in I2C addresses. It is also worth mentioning that the payload also had 4 other sensors not related to this study. These include two AS5600 magnetic encoders, a BME280 environmental sensor, and a BNO055 9-axis IMU. These sensors are part of a wind-direction and wind-speed sensor suite that was integrated into the payload structure. Although not directly used for analysis in the report, the BME280 also provided temperature, humidity, pressure, and altitude. The recorded altitude using the BME280 is used later in some plots. The BME280 has "±1 meter or better accuracy," "temperature with ±1.0°C accuracy," and also uses the I2C protocol [5]. Data from the BME280 was requested every 20ms (50Hz) and stored at the normal 1-second interval. In terms of power, a Lithium Ion polymer battery at 3.7V and 500mAh was used on the February flight, and a Lithium Ion polymer battery at 3.7V and 2000mAh was used on the April flight. To connect the electronics, 22 AWG wiring was used in conjunction with ELEGOO jumper ribbon cables. In total, with all the electronics, wiring, and insulation, the payload was 860g on the February flight and 968g on the April flight.

2.4. Uncertainty and Issues

To begin the uncertainty analysis, the limitations at which equipment can accurately record values are discussed. Many of the sensors used by the team are commercially available and manufacturers provide their estimated resolution and range. The first sensor, the INA219, is said to have a 12-bit ADC with ±3.2A range at 0.8mA. This can be changed to a more shallow ±400mA range at a 0.1mA resolution. Because the solar panels used in this study have a maximum rated current of 150mA, the team selected the more shallow ±400mA range. To measure the voltage, the datasheet only mentions a +26VDC voltage rating. Assuming a 12-bit ADC, the voltage resolution would then be about 0.006V. For simplicity, because the true resolution is unknown, and the sensor limitations are untested, the team assumed a 0.01V resolution similar to that of the current. More information regarding the limitations of these sensors can be found in the referenced documentation [2, 4].

Next, there is the VEML7700 luminosity sensor. As mentioned earlier, this sensor is also commercially available and has a "16-bit dynamic range for ambient light detection." To control this chip, the Adafruit_VEML7700.h library was used by the team. This library automates a great deal of the computation and it was difficult to sync the integration time (internal signal

amplification) with the main computer since code hanging would often occur. As a result, the VEML_LUX_CORRECTED_NOWAIT argument in the luxMethod function was used [6]. The documentation for this function is limited and it is assumed that the resolution is automatically adjusted by the chip during an I2C request. As a result, most of the data in this study was normalized by the team with respect to the max value for trend analysis rather than instantaneous values observation.

Finally, the team also wants to mention issues with the environment that may greatly affect the results. Because the payloads on high-altitude balloons are exposed to the environment for prolonged periods of time, environmental factors such as temperature, wind, and humidity may greatly affect the data collection process. As seen in Figure 6, during the February flight, the temperature inside the payload structure reached about -33 ℃ before shutting down the system. During this time frame, regardless of flight date, it is very well possible that other sensors and systems, such as the solar panel power modules, may experience anomalies due to the cold temperature. The team believes that it does not have enough experience with the sensors to truly de-couple the effects caused by the cold temperature with the efficiency of the INA219 power modules or the VEML7700 luminosity sensors. Another issue the team wanted to briefly address is the wind during the flight. Because the wind is constantly blowing on the payload, there is lots of rotation and sway. As such, it is very important to mount the solar panels in a way that is not only secure but also allows for constant access to the visible light coming from the sun.

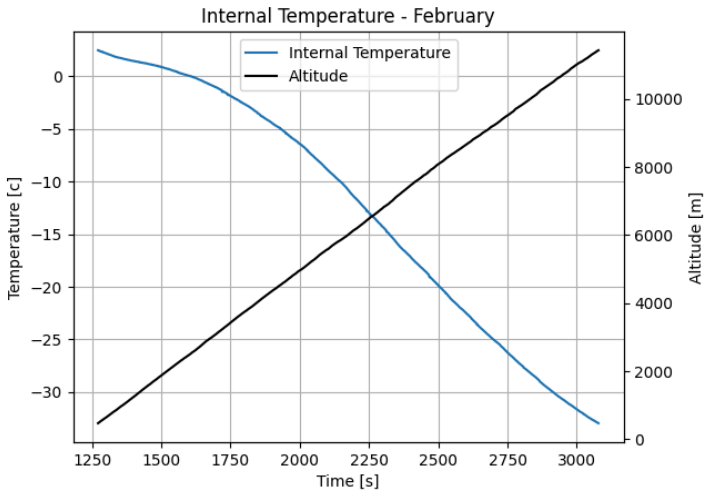

Fig. 6. Temperature of the internal electronics during the February 2024 test flight plotted against the flight time.

3. Results and Discussion

3.1. Solar Panel Voltages

As discussed earlier, there are a total of two flight opportunities that the team had to test the payload. The first flight and corresponding data set occurred on February 24. On this flight, the payload was launched from Kentland Experimental Aerial Systems (KEAS) Laboratory in Blacksburg, Virginia. The launch occurred at about 9:30 AM EST on a Kaymont 1600g balloon with 6 other payloads and was about 50 feet below the balloon. The next flight occurred on April 8th from Thayer High School in Thayer, Missouri. This was the 2024 total solar eclipse flight. The payload was mounted about 80 feet below the balloon and flew with 8 other payloads. A

Kaymont 2000g balloon was used and the launch occurred at about 12:30 PM CST. Before beginning the discussion, one last comment must be made regarding the coordinate system used in the analysis. When facing the payload structure, as seen in Figure 2, the left solar panel is defined as the one next to the anemometer while the right solar panel is defined as the one next to the wind vane as seen. This also applies to the luminosity sensors since they are mounted in-plane with the solar panels. In all subsequent plots, there will be some form of comment indicating which side of the structure the data was collected from.

Before applying any filtering to the data, the entire raw data can be seen in Figures 7-10 below. These plots are included for reference to show how the data set was scaled. Looking at the February data set, the flight began at roughly 1250 seconds and the battery drained at 3500 seconds. However, there was a confirmed wire fault on the main power system at 3100 seconds causing erroneous data measurements on all sensors. As such, for comparison, the data for only the time interval between 1250 and 3100 seconds is included in all future discussions of the February data. Next, the April data set can be examined. Looking at this data, there is a full eclipse at 5800 seconds. This coincides almost exactly with when the balloon landed back on the ground. Because the team is interested in only the ascent stage of the ballooning flight, this data is also trimmed to include only the interval between 400 and 3350 seconds. This modification in data set size allows for only the ascent stage of the high-altitude ballooning flight to be considered.

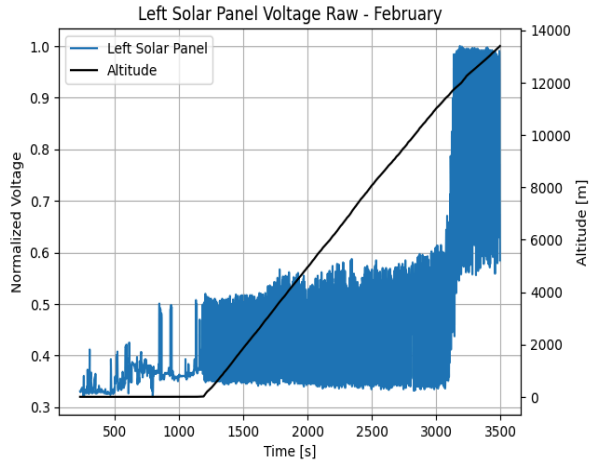

Fig. 7. Normalized voltage relative to the max value on the left solar panel versus time and altitude during the entire February flight.

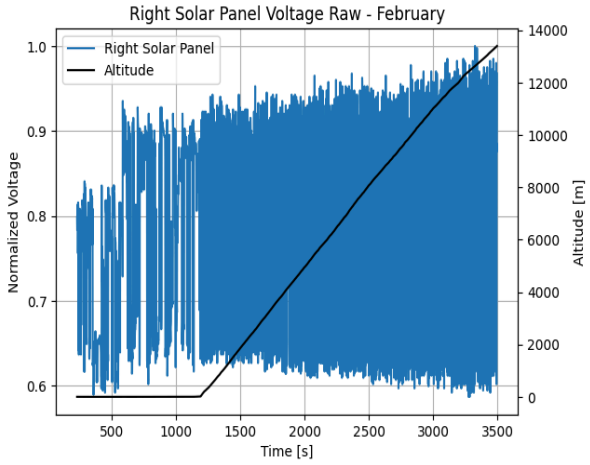

Fig. 8. Normalized voltage relative to the max value on the right solar panel versus time and altitude during the entire February flight.

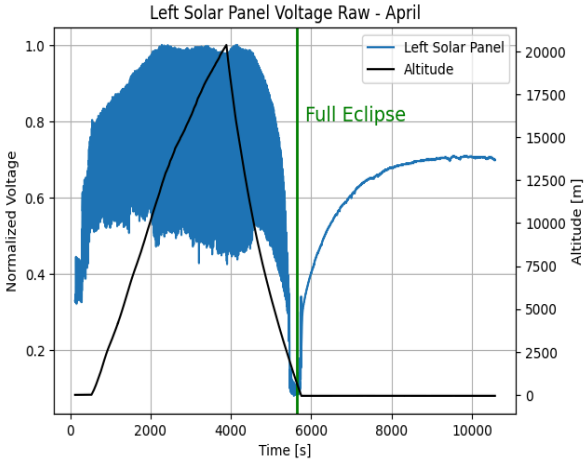

Fig. 9. Normalized voltage relative to the max value on the left solar panel versus time and altitude during the entire April flight.

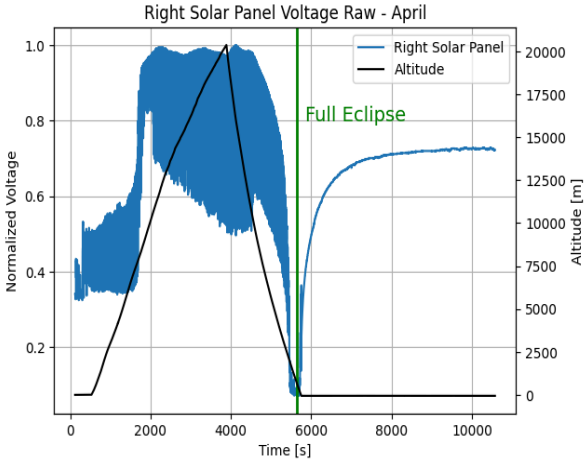

Fig. 10. Normalized voltage relative to the max value on the right solar panel versus time and altitude during the entire April flight.

Based on these plots, the raw trimmed data can be visualized in Figures 11-14 below. The y-axis on the left represents the normalized voltage relative to the maximum value recorded while the right y-axis represents the calculated altitude from barometric pressure by the BME280 sensor. Looking at the graphs, the data looks very noisy. Due to the rotational motion of the payload structure, the solar panels would be facing the sunlight at one instant but then rotate away shortly after. As such, the data has a "sinusoidal" like movement when analyzed closely. Another observation can be made about the right solar panel on the April flight. Although post-analysis results do not show damage to the circuit, it is very likely that some sort of open-circuit event occurred 1600 seconds into the flight. This can be further supported by Figure 24 which shows a rapid decrease in current (i.e., increase in voltage). The team opted to include these results in the following discussions because they can still be used to observe the general trends related to the solar panel during flight and cutting the data at the fault would more than half the entire dataset for the April flight.

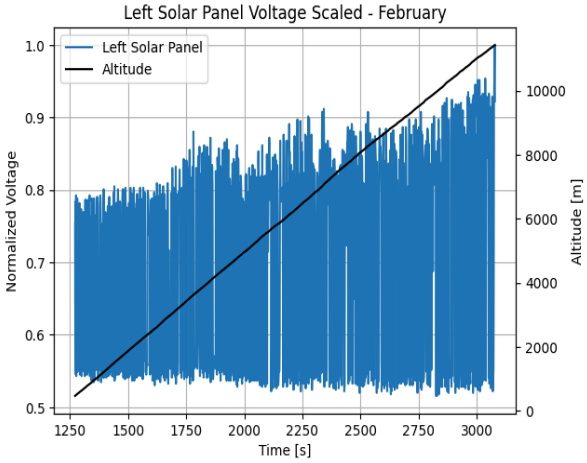

Fig. 11. Normalized voltage relative to the max value on the left solar panel versus time and altitude during the scaled February flight.

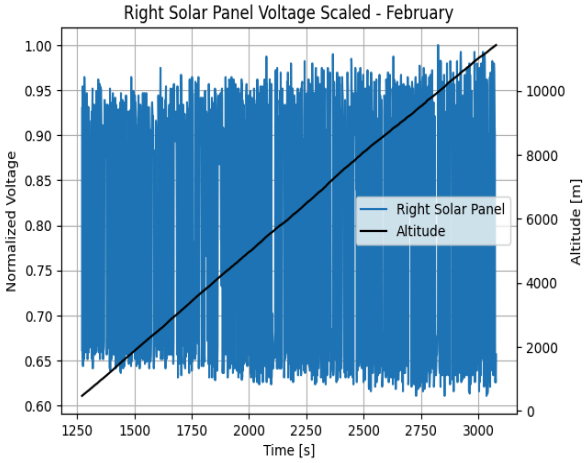

Fig. 12. Normalized voltage relative to the max value on the right solar panel versus time and altitude during the scaled February flight.

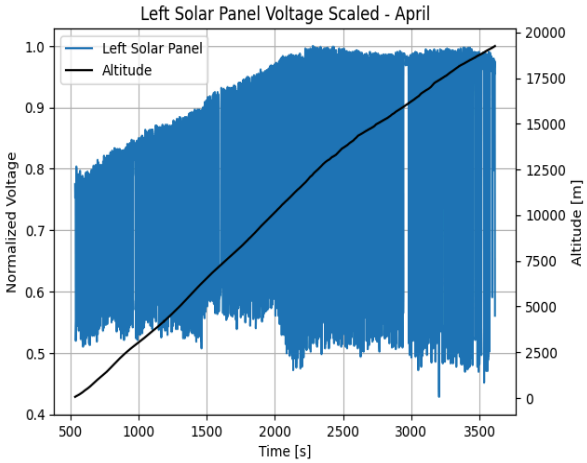

Fig. 13. Normalized voltage relative to the max value on the left solar panel versus time and altitude during the scaled April flight.

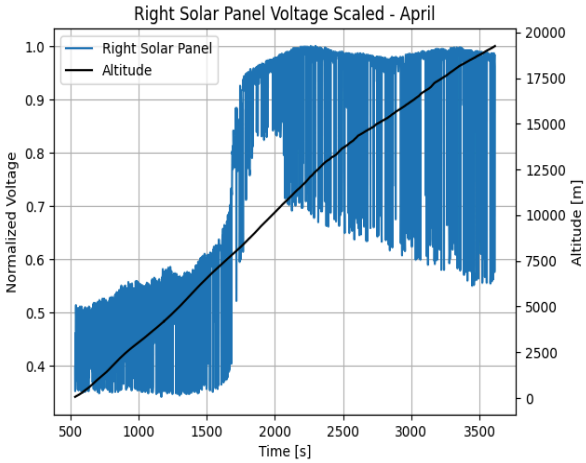

Fig. 14. Normalized voltage relative to the max value on the right solar panel versus time and altitude during the scaled April flight.

The first thing the team did to help analyze this data was implement a moving average filter to the data set. The moving average filter worked by summing up the last 120 data points (2 minutes) and dividing by the total number of data points (120). This was done in a "rolling" fashion so that every data point was averaged. Equation (1) below shows the mathematical representation of the moving average filter used:

$$y[i] = \frac{1}{M} \sum_{j=0}^{M-1} x[i + j] \tag{1}$$

Where M is the number of data points that would be averaged, i is the output signal index, and j is the summation index. To implement this feature in Python, a convolution function was used to merge, sum, and divide the datasets [7].

The results of this filter can be seen in Figures 15 and 16. In these figures, the sinusoidal-like motion is observed. As one solar panel faces away from the sun the other solar panel receives sunlight. This is visible at 2250 seconds into the February flight. As the right solar panel faces away from direct sunlight and experiences a decrease in voltage the left solar panel experiences an increase in voltage. If compared to a sinusoidal wave, the phase difference between these two panels would be around 180 degrees.

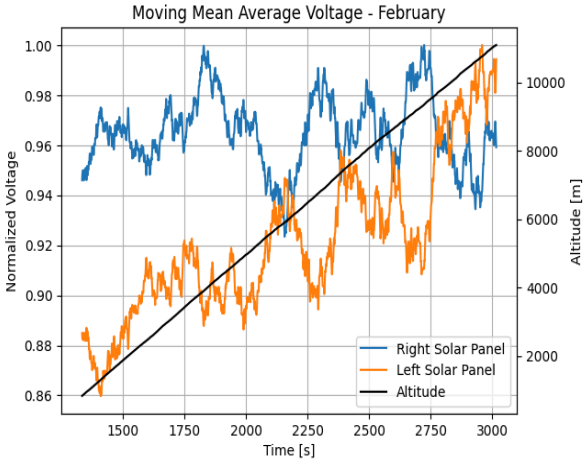

Fig. 15. Moving mean plot of the normalized voltage relative to its local maximum value on the left and right solar panel versus time and altitude during the February flight.

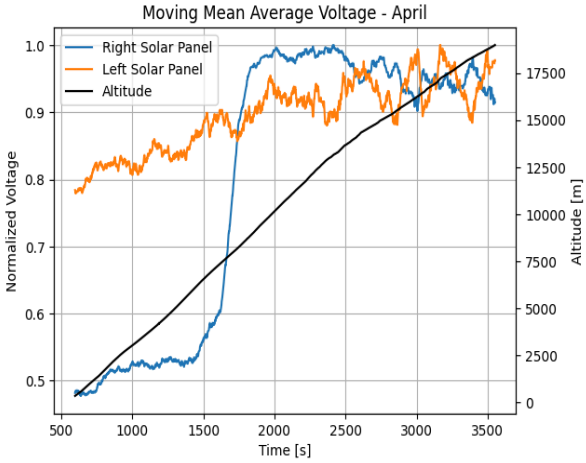

Fig. 16. Moving mean plot of the normalized voltage relative to its local maximum value on the left and right solar panel versus time and altitude during the April flight.

Another technique the team used to measure trends is by implementing a linear regression algorithm to the data values. A linear regression algorithm is a statistical method that fits a linear relationship to the data values. This linear regression algorithm was once again applied to the raw data and resulted in the trends seen in Figures 17-20 below. Based on the algorithm, the computed R-squared values for the left solar panel and right solar panel were 0.16 and 0.01 for the February flight and 0.24 and 0.74 for the April flight.

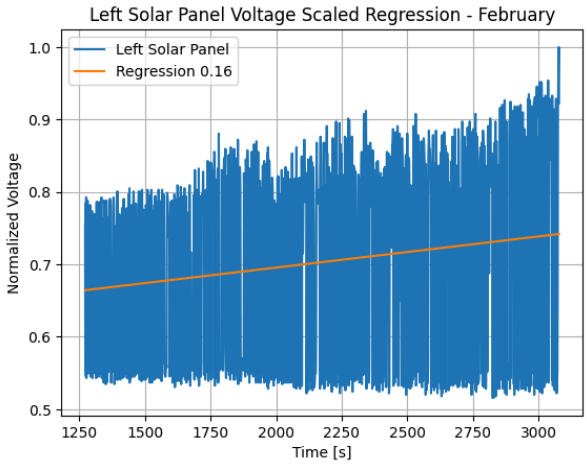

Fig. 17. Normalized voltage relative to the max value on the left solar panel versus time for the February flight. Linear regression fitted to the dataset and plotted in orange.

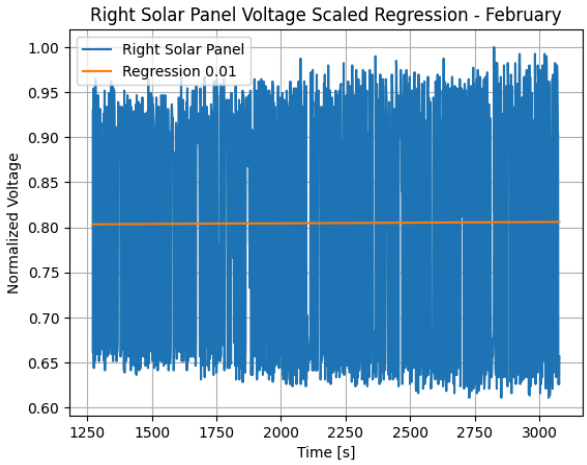

Fig. 18. Normalized voltage relative to the max value on the right solar panel versus time for the February flight. Linear regression fitted to the dataset and plotted in orange.

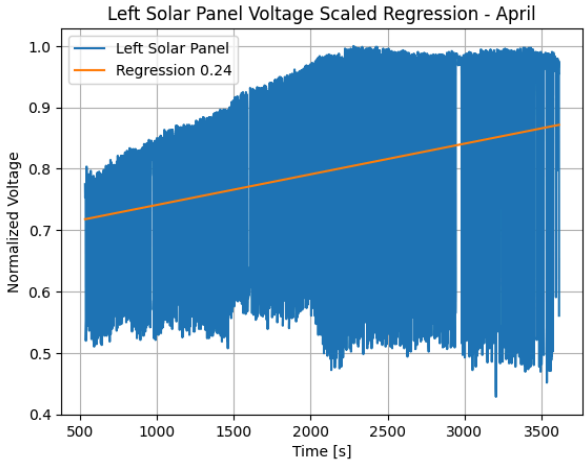

Fig. 19. Normalized voltage relative to the max value on the left solar panel versus time for the April flight. Linear regression fitted to the dataset and plotted in orange.

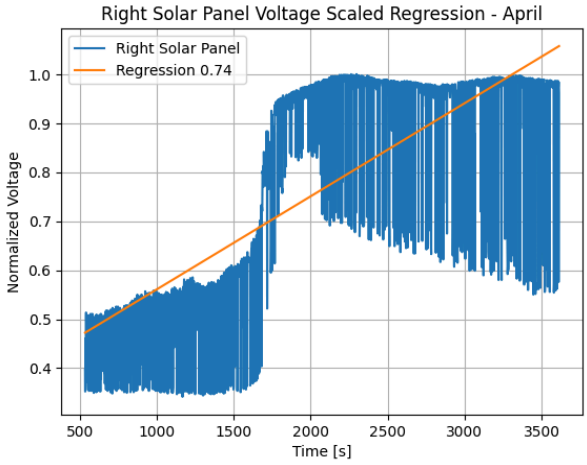

Fig. 20. Normalized voltage relative to the max value on the right solar panel versus time for the April flight. Linear regression fitted to the dataset and plotted in orange.

3.2. Solar Panel Currents

The next data that is of interest is the corresponding solar panel current during the flight. As mentioned in section 3.1, the data related to the current was also trimmed to include only the relevant intervals. Figures 21-24 show the plotted current during the flight. The left y-axis represents the normalized current relative to the max value while the right side y-axis represents the altitude in meters. Looking at the data, it looks very similar to that of the voltage. However, when compared to the trends in voltage, the current is less oscillatory and never goes beyond a minimum value of 0.

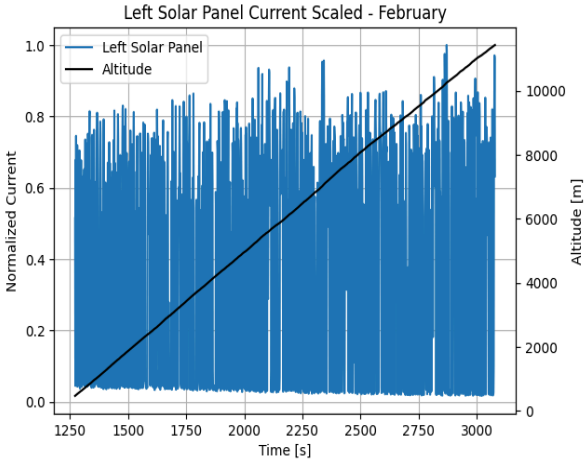

Fig. 21. Normalized current relative to the max value on the left solar panel versus time and altitude during the scaled February flight.

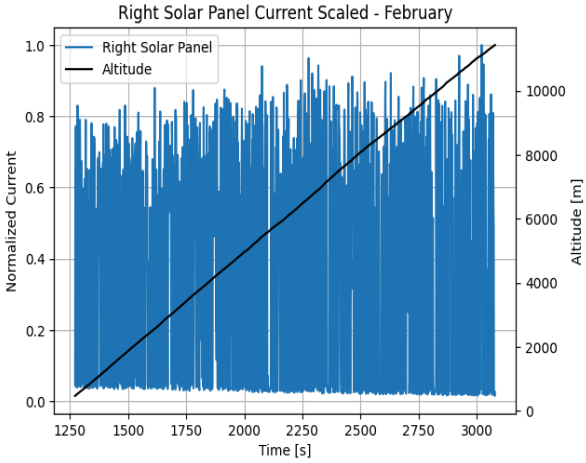

Fig. 22. Normalized current relative to the max value on the right solar panel versus time and altitude during the scaled February flight.

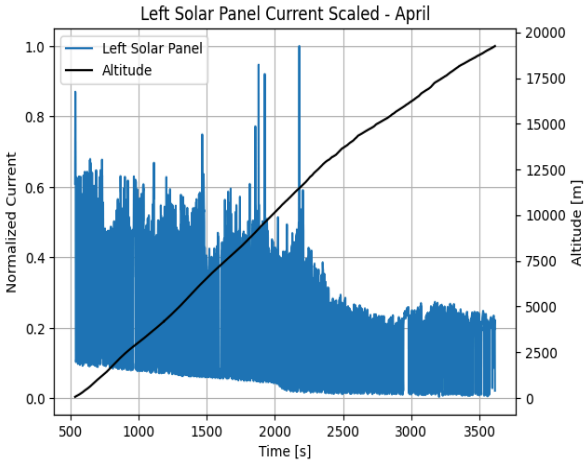

Fig. 23. Normalized current relative to the max value on the left solar panel versus time and altitude during the scaled April flight.

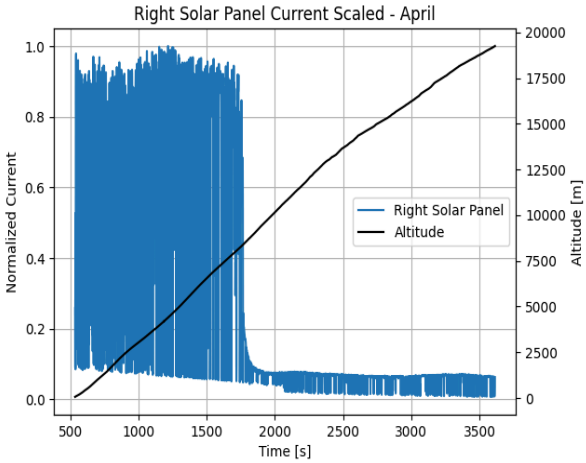

Fig. 24. Normalized current relative to the max value on the right solar panel versus time and altitude during the scaled April flight.

Applying a moving average filter to the most recent 120 data points yields Figures 25 and 26. Similar to the voltage trends in Figures 15 and 16, these plots demonstrate an oscillatory behavior. As one solar panel is away from the sun and records a local minimum value the opposite solar panel is in the sun and records a local maximum value.

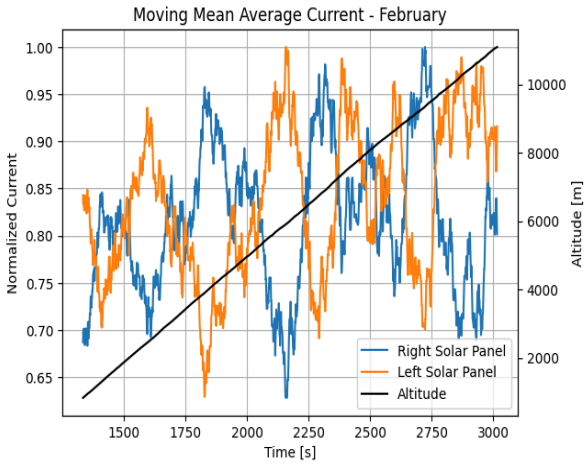

Fig. 25. Moving mean plot of the normalized current relative to its local maximum value on the left and right solar panel versus time and altitude during the February flight.

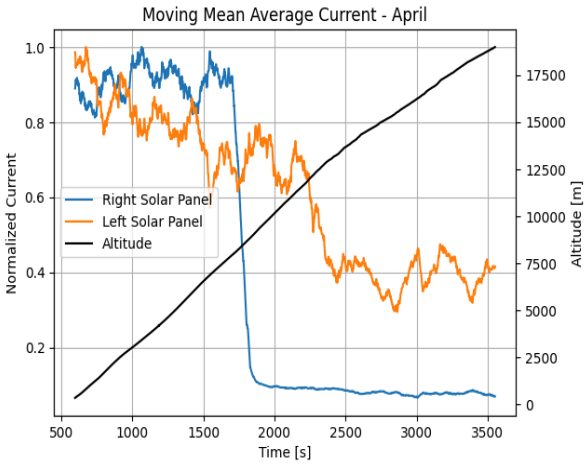

Fig. 26. Moving mean plot of the normalized current relative to its local maximum value on the left and right solar panel versus time and altitude during the April flight.

Just like in section 3.1, another way to interpret this data is by applying a linear regression algorithm. As expected, the linear regression shows a positive upward trend for the February data and a negative downward trend for the April data due to the decrease in available sunlight during the eclipse. Figures 27-30 show this trend and corresponding R-squared values.

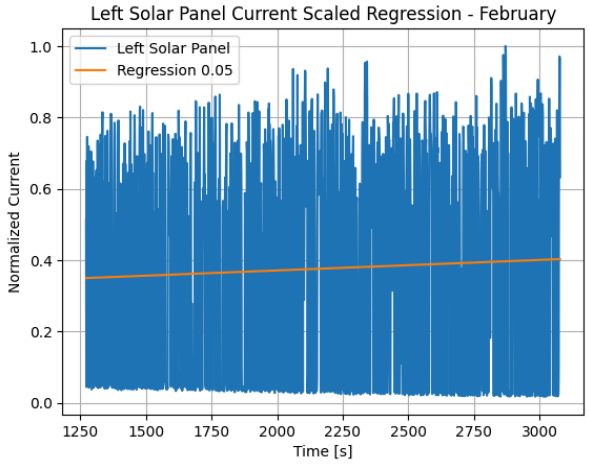

Fig. 27. Normalized current relative to the max value on the left solar panel versus time for the February flight. Linear regression fitted to the dataset and plotted in orange.

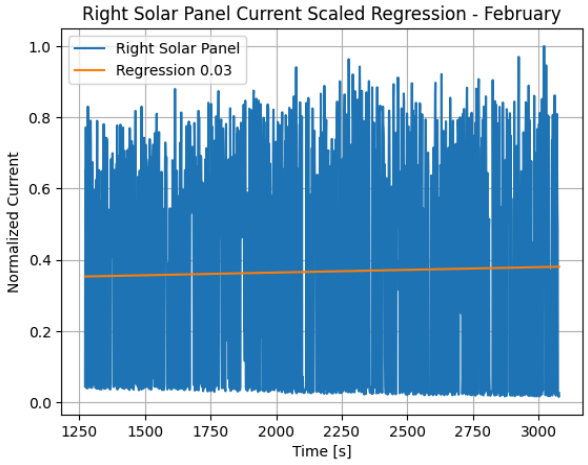

Fig. 28. Normalized current relative to the max value on the right solar panel versus time for the February flight. Linear regression fitted to the dataset and plotted in orange.

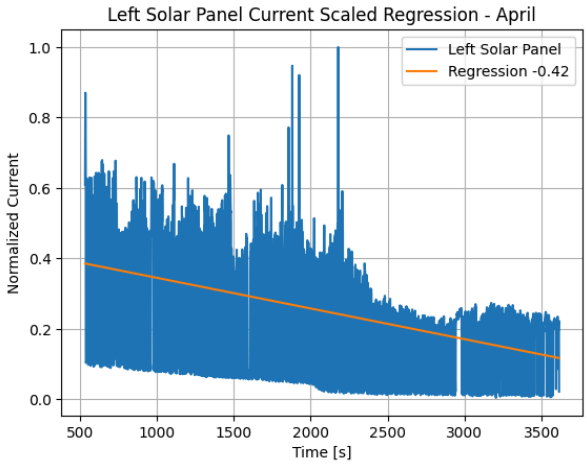

Fig. 29. Normalized current relative to the max value on the left solar panel versus time for the April flight. Linear regression fitted to the dataset and plotted in orange.

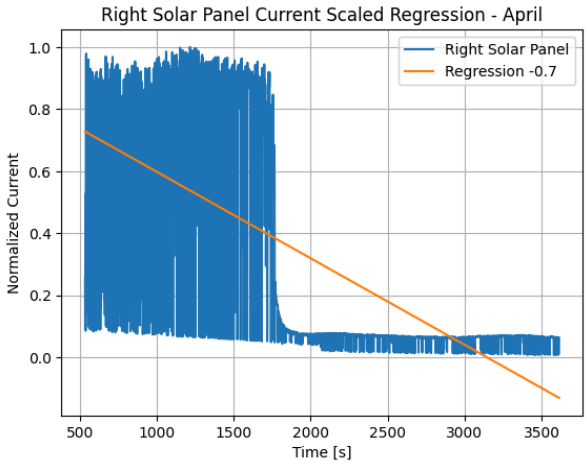

Fig. 30. Normalized current relative to the max value on the right solar panel versus time for the April flight. Linear regression fitted to the dataset and plotted in orange.

3.3. Luminosity Values

The last data variable that is of interest is the luminosity recorded by the VEML7700 sensor during the flight. The luminosity data set is also trimmed to the interval of interest and the value is normalized to the recorded maximum value. For the sake of simplicity, only the moving average and linear regression figures are provided. Examining Figures 31-34, the luminosity sensors show a very similar trend to that seen in Figures 27-30 for the recorded current. As such, it seems that the current and luminosity are almost directly proportional in their trend when it comes to their normalized values against altitude.

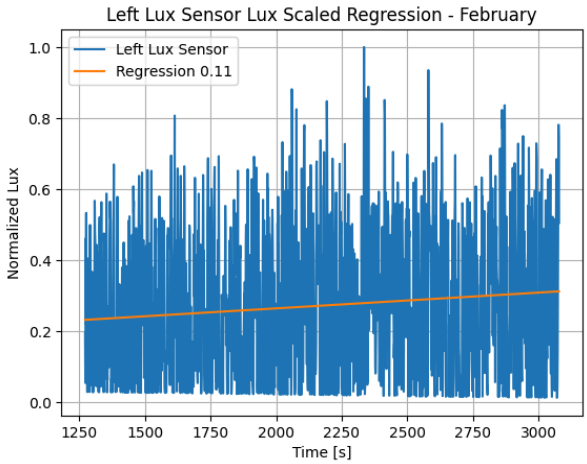

Fig. 31. Normalized luminosity relative to the max value on the left solar panel versus time for the February flight. Linear regression fitted to the dataset and plotted in orange.

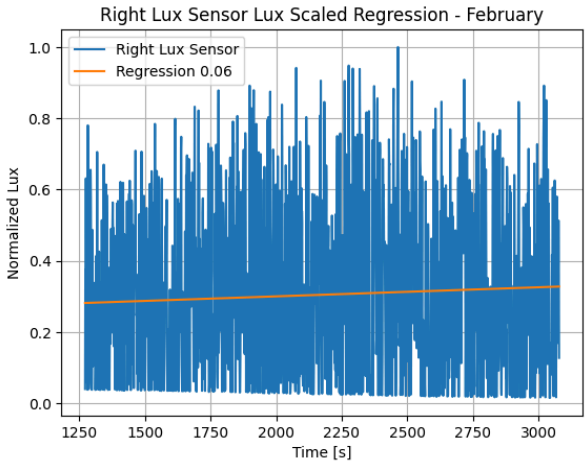

Fig. 32. Normalized luminosity relative to the max value on the right solar panel versus time for the February flight. Linear regression fitted to the dataset and plotted in orange.

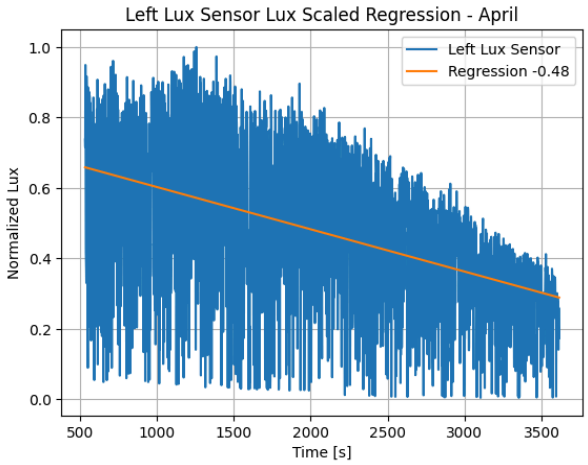

Fig. 33. Normalized luminosity relative to the max value on the left solar panel versus time for the April flight. Linear regression fitted to the dataset and plotted in orange.

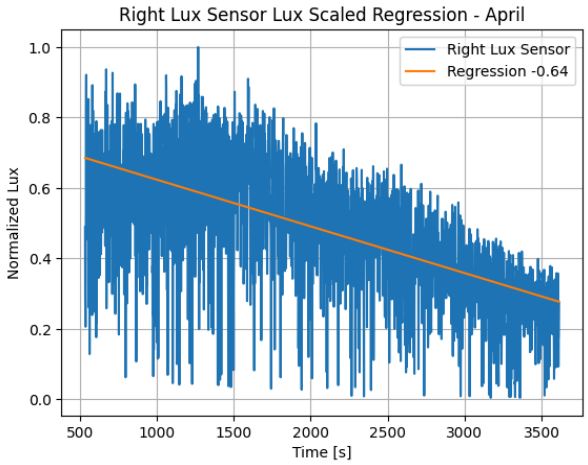

Fig. 34. Normalized luminosity relative to the max value on the right solar panel versus time for the April flight. Linear regression fitted to the dataset and plotted in orange.

Finally, Figures 35 and 36 show the implementation of the moving average filter to the values. Once again, the moving mean average shows an oscillatory behavior and a linearly increasing trend with respect to the recorded altitude.

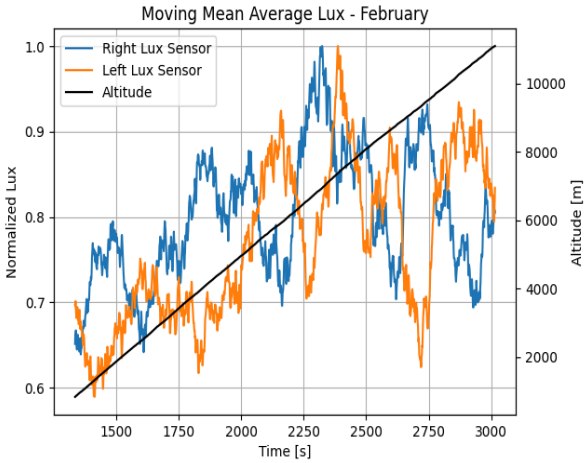

Fig. 35. Moving mean plot of the normalized luminosity relative to its local maximum value on the left and right solar panel versus time and altitude during the February flight.

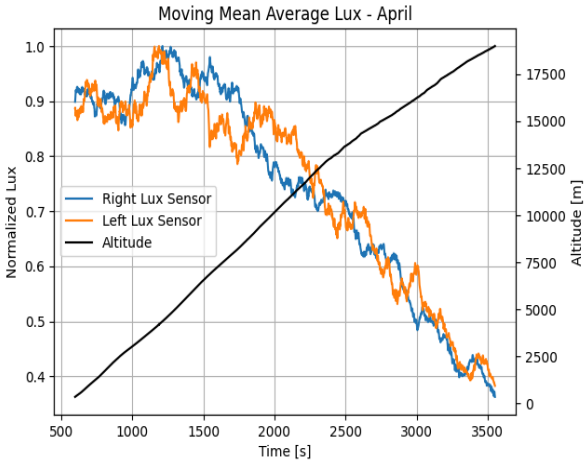

Fig. 36. Moving mean plot of the normalized luminosity relative to its local maximum value on the left and right solar panel versus time and altitude during the April flight.

4. Conclusion

An experiment has been performed by members of the HAB@VT design team to determine how the recorded voltage and current across a solar panel change over the duration of the ascent stage of a high-altitude balloon flight. Two datasets were examined for two different consumer-grade

polycrystalline solar panels of 2.36-inch by 3.54-inch size. The first dataset was obtained during a flight on February 24, 2024, while the second dataset was obtained from a flight on April 8, 2024. The data was very oscillatory in nature due to the rotational motion of the payload structure caused by the wind and other environmental factors. To filter out the noise and visualize the underlying trends, a moving average filter was applied to the dataset. Linear regression was also performed to obtain a general trend of the data. Based on the analysis of this data, the team was able to make the following conclusions.

As the altitude increases during a high-altitude balloon flight, the corresponding voltage on both the left and right solar panels also slowly increases assuming light conditions do not change. Additionally, the amount of current produced by the solar panels is almost directly related to the amount of sunlight detected by the luminosity sensors. This supports the current research related to the effects of light intensity on power production [8]. Comparing Figures 27-34 shows that as the brightness increases, the amount of current produced by the solar panels also increases. Another notable conclusion is that general trends indicate solar panels can function effectively on high-altitude balloons. The data indicates that the efficiency (voltage and current levels) does not decrease during the ascent stage of the flight and, instead, actually increases. This supports current research suggesting that cold weather improves the efficiency of solar panels [9]. Finally, although easy to implement, considerations must be taken regarding the mounting and arrangement of the solar panels. Due to wind and other environmental factors, rotational motion is introduced to payloads secured to a flight string. As such, the power produced by the solar panels is sinusoidal as a solar panel rotates towards and away from the sun. The team believes this issue may be resolved by integrating batteries, capacitors, or other energy storage methods in conjunction with the solar panels.

Acknowledgments

The team is extremely grateful for the support it received during this research study. This includes the Kevin T. Crofton Department of Aerospace and Ocean Engineering and the Bradley Department of Electrical and Computer Engineering at Virginia Tech. The team would also like to acknowledge Virginia Space Grant Consortium Award #23-162-100846-010. Finally, the team is thankful for the mentorship and guidance provided by Kevin Sterne and Virginia “Ginny” Smith for the duration of the study.

References

1 “Polycrystalline vs monocrystalline solar panels: What’s the difference?,” OneMonroe, https://monroeengineering.com/blog/polycrystalline-vs-monocrystalline-solar-panels-whats-the-difference/ (accessed May 17, 2024).
2 K. “High Accuracy Ambient Light Sensor with I2C Interface,” Vishay, https://www.vishay.com/docs/84286/veml7700.pdf (accessed May 17, 2024).
3 “Adafruit Right Angle VEML7700 Lux Sensor - I2C Light Sensor - STEMMA QT / Qwiic,” Adafruit, https://www.adafruit.com/product/5378 (accessed September 27, 2024).
4 lady ada, “Adafruit INA219 Current Sensor Breakout,” Adafruit Industries, https://cdn-learn.adafruit.com/downloads/pdf/adafruit-ina219-current-sensor-breakout.pdf (accessed May 17, 2024).
5 “Adafruit BME280 I2C or SPI Temperature Humidity Pressure Sensor - STEMMA QT,” Adafruit, https://www.adafruit.com/product/2652 (accessed May 17, 2024).

6 Adafruit, "Adafruit VEML7700 Lux Sensor Library," GitHub, https://adafruit.github.io/Adafruit_VEML7700/html/_adafruit___v_e_m_l7700_8h.html (accessed May 17, 2024)
7 R. Oshana, “Moving Average Filters,” in The Scientist & Engineer’s Guide to Digital Signal Processing, San Diego, California, 1999, pp. 277–284.
8 J. Amajama, “Effect of Solar ILLuminance (or Intensity) on Solar (Photovoltaic) cell's output and the use of Converging lenses and X or Gamma rays to enhance output performance,” in International Journal of Engineering Research and General Science, July-August, 2016, Volume 4, Issue 4, pp. 284-289.
9 Rk Naresh, “Re: Does cold temperature affect solar panel efficiency and which solar panel is best for high temperature and solar panels work in rainy weather?,” ResearchGate, 2023, https://www.researchgate.net/post/Does_cold_temperature_affect_solar_panel_efficiency_and_which_solar_panel_is_best_for_high_temperature_and_solar_panels_work_in_rainy_weather/655afdeb6e3206f5e2083330/citation/download (accessed May 17, 2024).